Materials Advances

ROYAL SOCIETY OF CHEMISTRY

PAPER

View Article Online
View Journal | View Issue

Cite this: *Mater. Adv.*, 2022, 3, 7925

A fluorescent Ce-EDTA probe for the sensing of ascorbic acid and lysine in real samples

Rajpal, Ashish Kumar, Subhajit Jana, Priya Singh and Rajiv Prakash *

Received 28th April 2022,
Accepted 10th August 2022

DOI: 10.1039/d2ma00477a

rsc.li/materials-advances

In the present work, a fluorescent probe based on an aqueous dispersion of coordination complex Ce-EDTA is utilized for sensing carboxyl compounds. Ce-EDTA is synthesized herein by a hydrothermal method with the help of stoichiometric ratios of cerium (Ce) (+III) salts and green ligand ethylenediamine *N,N,N,N* tetra-acetic acid (EDTA). In Ce-EDTA, the Ce ion is surrounded by hexadentate EDTA and three labile aqua ligands, evidenced by FT-IR, XPS, and UV-visible spectroscopy. It exists in the form of polygonal microplates, as apparent by SEM. The sensing mechanism is proposed by choosing carboxyl groups as a part of the ring and open chain. Under the optimized situations, the fluorescence intensities of Ce-EDTA are monitored towards various concentrations of L-lysine (Lys) and ascorbic acid (AA) in these regards. They exhibit a linear response from 20.29 μM to 251.74 μM and 5.62 μM to 60.87 μM with a linear correlation coefficient (R^2) of 0.98 and 0.99, respectively. The lower limit of detection is observed as 3.6 μM in the case of Lys and 2.04 μM in the case of AA. The as-prepared probe exhibits suitability for selectivity of AA and Lys in the presence of various interfering agents as well as in real samples for the detection of AA in orange and Lys in soybean seed.

1. Introduction

Ascorbic acid (AA), recognized as vitamin C, is a crucial water-soluble molecule.[1,2] However, it is not produced in the human body[3] and is sourced mainly from fresh vegetables and fruits.[4] It is an essential nutrient material with a highly reducing character, which conveys excellent capability for cancer prevention, scavenging free radicals, and encouraging iron absorption.[5,6] In addition, it also plays a vital role in preserving the human body's regular metabolism and physiological system,[7,8] along with the biological and chemical circumstances, pharmaceutical engineering, and nutritional systems.[9,11] However, an insufficiency of AA is responsible for numerous diseases like cancer, cardiovascular disease, and especially the famous scurvy.[7,12–14] The recommended dietary allowance (RDA) of AA intake is 70–90 mg per day, which can prevent scurvy.[15,16] Recent studies also suggest that an AA dose greater than 500 mg per day positively affects endothelial function.[12,13] At the same time, excess AA intake, more than 2000 mg per day, results in urinary stones,[17,18] diarrhea, and stomach cramps.[10,19–21] In an optimal quantity, it is also used for mental sickness therapeutics, improving immunity, and treating the common cold, infertility, and cancer.[4] Therefore, monitoring the AA level in natural foods and supplementary food tablets, and their systematic intake is highly desirable for successful therapeutic strategies. L-Lysine (Lys) is an essential amino acid that is not only beneficial for increasing immunity but also used as a fat burner. The average intake in humans is 4–5 g per day.[22] In addition, excess Lys in human urine and blood causes abnormal metabolic problems, *e.g.*, cystinuria[23] or hyperlysinaemia.[24] Lys in human urine is a signature of damage in liver functioning. Similarly, a deficiency of Lys causes hair loss, fatigue, anemia, inflamed eyes, distorted and stunted growth, and reproductive complications.[25] Therefore, monitoring AA and Lys is highly desirable.

Among the various methods, the fluorescent method is a very satisfying method for sensing such kinds of analytes based on fluorescent probes due to their high reliability and sensitivity. Cerium is one of the most abundant rare-earth metals from the lanthanide series, of which only 0.0046% is accessible on the earth's crust by weight.[26] That is why it could be a part of fluorescent probes from an economic point of view. Herein, cerium(III) ions are generally used in various analytical techniques due to their two utmost stable oxidation states (Ce^{3+} and Ce^{4+}), which approve the several geometries having coordination numbers from 8 to 10.[27,28] In addition, the Ce^{3+} is accountable for the best fluorescent properties, especially in Ce(III)-based coordination polymeric form, over Ce^{4+} due to the vacant 4f orbital.[28–30] On the other hand, the luminescent properties of Ce-based coordination complexes are strongly influenced by the specific organic ligands and the coordination manner. The organic ligands have the leading role in managing the ligand field effect that assists the absorption of light to create enough photons. Moreover, Ce ions can also be sensitized with acceptable antenna ligands, which are sheltered

School of Materials Science and Technology, Indian Institute of Technology (Banaras Hindu University), Varanasi, India. E-mail: rprakash.mst@iitbhu.ac.in

from the process of nonradiative deactivation.[27] In continuation, in particular, the sensing properties are attributed to the reactions between additive analytes and the luminescent probe that lead to evident variations in the luminescence phenomenon as emission enhancement or quenching. Similarly, as a coordinating ligand, ethylenediaminetetraacetic acid (EDTA) is generally considered one of the riveting applicants for gathering metal–organic coordination complexes or polymers due to its several oxygen and nitrogen chelating sites and flexible bonding manner.[31–33] EDTA-based coordination complexes have been demonstrated to play central roles in various applications like catalysis,[34] magnetics,[35] and toxic metal ion recognition.[36] In these views, we synthesized a Ce(III)-EDTA complex by a facile hydrothermal process and used it to prepare a fluorescent probe for sensing molecules having carboxyl moieties in the presence of various interferents. Herein, the carboxyl functionality was intentionally chosen as a part of a closed ring (as in AA) and open chain (as in Lys) to justify our sensing mechanism. The as-synthesized fluorescent probe is characterized by ultraviolet-visible (UV-Vis), Fourier transforms infrared (FT-IR) spectroscopy, X-rays diffraction (XRD), and scanning electron microscopy (SEM) for its structural and morphological analysis. The probe is further successfully applied for recognizing AA in commercially available ascorbic acid tablets, orange juice, and Lys in soybean seeds.

2. Experimental

2.1 Materials

Cerium(III) nitrate hexahydrate [Ce $(NO_3)_3{\cdot}6H_2O$] (99%), D-(+)-glucose anhydrous ($C_6H_{12}O_6$) (99.5%), and L-lysine ($C_6H_{14}N_2O_2$) (98–103%) were purchased from HIMEDA, India. Sodium hydroxide pellets (NaOH) (97%) and sodium chloride (NaCl) (99%) were obtained from Merck, India. Ethylenediaminetetraacetic acid (EDTA) [$C_{10}H_{16}N_2O_8$] (99.4%) was purchased from LOBA Chem, India. L-Ascorbic acid (vitamin C) ($C_6H_{18}O_6$) (99.7%) was purchased from SDFCL, India. Magnesium nitrate hexahydrate ($MgN_2O_6{\cdot}6H_2O$) (98%) and L-glutathione ($C_{10}H_{17}N_3O_6S$) (98%) were from Sigma-Aldrich, and L-cysteine ($C_3H_7NO_2S$) (99%), lactose ($C_{12}H_{22}O_{11}{\cdot}H_2O$) (99.8%) and D-fructose ($C_6H_{12}O_6$) (99.7) were purchased from SRL, India. The above chemicals were utilized without any external refinement.

2.2 Instrumentation

Ultraviolet-visible (UV) spectra were recorded using solid complexes on a SHIMADZU UV-VIS spectrophotometer (UV-2600), and photoluminescence (PL) spectra were noted using a stable aqueous dispersion of Ce-EDTA complex on F-4600 FL Spectrophotometers. Fourier transform infrared (FT-IR) spectroscopy was recorded on a Thermo Scientific NICOLET iS5 instrument from 500 cm^{-1} to 4000 cm^{-1}. Scanning electron microscope (SEM) images were taken on an EVO-scanning electron microscope MA 15/18 instrument. X-Ray photoelectron spectroscopy (XPS) measurement was performed on a Thermo Fischer Scientific ESCALAB Xi +.

2.3 Synthesis of the Ce-EDTA complex

The Ce-EDTA complex is synthesized by a hydrothermal process.[31,32] In this process, 0.125 molars (735 mg) of EDTA ($C_{10}H_{16}N_2O_8$) were first solubilized in 10 ml of DI water, and then 0.67 molars (276.28 mg in 10 ml DI water) of sodium hydroxide solution were also added (pH = 6) to it with continuous stirring. Thereafter, 0.1 molar (877.21 mg) Ce $(NO_3)_3{\cdot}6H_2O$ was prepared in DI water and added to the above reaction mixture under continuous stirring. After 30 minutes, the as-obtained white precipitate is transferred into a 30 ml Teflon-coated autoclave vessel, sealed, and heated at 180 °C for 24 h. The as-synthesized Ce-EDTA complex was washed with DI water and then ethanol consecutively and dried at 80 °C. Finally, Ce-EDTA is annealed in the presence of nitrogen gas in a tubular furnace at 180 °C temperature and kept for further use.

3. Results and discussion

It has been observed that the sensing analyte can replace coordinated water, resulting in a decrease in the fluorescence intensity due to the delocalization of L ← M charge transfer towards the analytes.[37,38] Sometimes, analyte molecules/ions are also able to interact with the reactive end of ligands coordinated with central metal ions, which results in an increase in the fluorescence spectrum due to the localization of L → M charge transfer towards the metals.[39–43] That is why we are expecting the formation of a 9-coordinated complex as per chemical reactions stated in the synthesis section and shown schematically in Fig. 1a.[44–47] Based on these speculations, further explanation is extended later in the sensing section by choosing the carboxyl group as a part of the ring (as in AA) and an open chain (as in Lys).

3.1 Structural analysis

The structural analysis of the Ce-EDTA complex is analyzed by XRD and compared with diffraction peaks of pure EDTA. XRD of EDTA exhibits its characteristic diffraction peaks; however, on complexation with Ce^{3+}, these peaks slightly shifted to lower 2θ values. All the diffraction peaks found in the XRD patterns confirm the formation of mixed-phase both in EDTA and Ce-EDTA.[31] In order to validate these phases present in both the compounds, we used FullProf.2k software for XRD profile matching & integrated intensity refinement (Fig. 1b and c). All the structural parameters like lattice parameters and lattice volume found from the Le Bail profile fitting are summarized in Table 1. It has been found that the simulated patterns are well-matched with the experimental data of either compound. EDTA has been found to consist of two phases with lower symmetry, *i.e.*, monoclinic and triclinic crystal phases having space groups '$C2/c$' and '$P\bar{1}$', respectively. Similarly, Ce-EDTA is composed of one monoclinic phase having space group '$P2_1/n$' and one triclinic phase with space group '$P\bar{1}$'. The crystal volume of

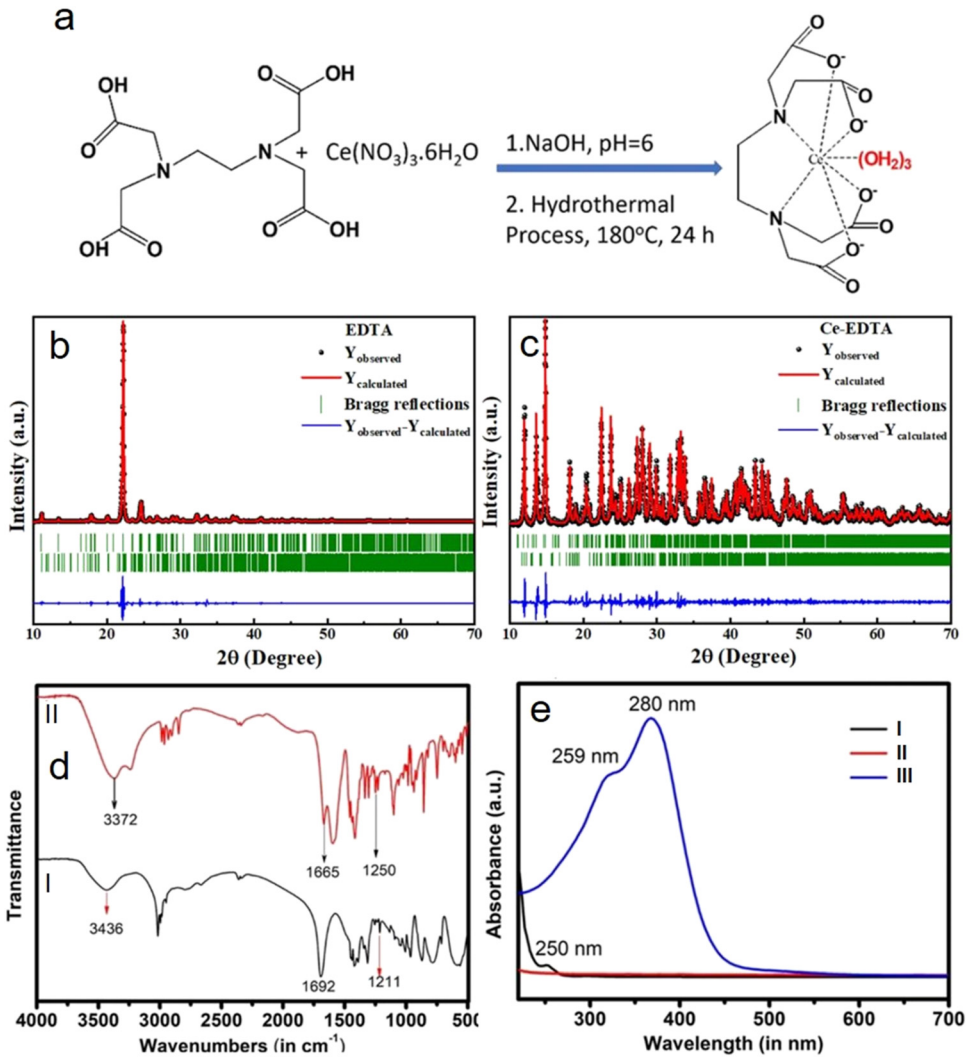

Fig. 1 (a) Schematic chemical reaction for the formation of the Ce-EDTA complex, XRD pattern fitted with Le Bail profile matching & integrated intensity refinement of (b) EDTA and (c) the Ce-EDTA complex, (d) FT-IR of (I) EDTA and (II) Ce-EDTA and (e) UV visible spectra of (I) cerium nitrate, (II) EDTA and (III) the Ce-EDTA complex.

Table 1 Crystal lattice parameters for EDTA and Ce-EDTA

	EDTA		Ce-EDTA	
Structural parameters	Phase 1	Phase 2	Phase 1	Phase 2
Phase	Monoclinic	Triclinic	Monoclinic	Triclinic
Space group	$C2/c$	$P\bar{1}$	$P2_1/n$	$P\bar{1}$
a (Å); b (Å); c (Å)	13.31; 5.61; 16.15	7.67; 8.17; 13.51	9.22; 16.10; 11.98	7.51; 7.82; 14.04
Volume (Å^3)	1197.66	816.71	1777.085	798.458
α (°); β (°); γ (°)	90.0; 96.36; 90.0	79.59; 81.95; 80.58	90.0; 92.73; 90.0	79.06; 83.06; 82.00
χ^2	5.6		2.92	

Ce-EDTA in its monoclinic phase is increased and in the triclinic phase is decreased as compared to pure EDTA due to the coordination of ligands during complex formation.

The chemical functionalities of the as-synthesized complex were analyzed by FT-IR spectroscopy (Fig. 1d). Except for a few changes in vibration frequencies (lowering of vibration frequency), both EDTA and the Ce-EDTA complex exhibit almost similar spectra (*cf.* Fig. 1d(I) and (II)). These changes, especially towards lower vibration frequencies, are direct consequences of complex formation.[1] For example, EDTA exhibits a vibration peak at 3436 cm^{-1} corresponding to O–H stretching associated with hydrogen-bonded -COOH. However, it vanishes and exhibits O–H vibration at a new position (3372 cm^{-1}) corresponding to water-coordinated ligands, as shown in Fig. 1a above.[48,49]

The EDTA has C═O stretching vibration corresponding to –COO^- at 1692 cm^{-1}, which has further shifted to 1665 cm^{-1} when complexation with Ce^{3+} occurs. Similarly, EDTA shows intense vibration at 1211 cm^{-1}, corresponding to aliphatic C–N stretching, which has shifted to 1250 cm^{-1}. The evidence for complex formation was further justified by UV-Visible analysis, as shown in Fig. 1e. It is evident that Cerium nitrate gives an absorption peak at 250 nm due to the 4f → 5d transition (Fig. 1e(I)).[20] EDTA has no absorption spectra in the given range of wavelengths, whereas on complexation as Ce-EDTA, two absorption peaks are observed at 259 nm, and 280 nm due to 4f → 5d spin allowed transitions.[50] In comparison to that of the free Ce^{3+} ion, the redshift of the absorption peak specifies a crystal-field effect on the 5d orbitals of the Ce^{3+} due to complexation (*cf.* Fig. 1e(II) and (III)).[51]

The bonding state of all available elements in the Ce-EDTA complex was analyzed by XPS (Fig. 2). First, the presence of all possible elements was observed by the survey spectrum (as shown in Fig. 2a) and then the corresponding peaks are deconvoluted to specify the bonding states of the concerned elements. The survey spectrum was evaluated for the existence of C1s (50.44%), N1s (9.24%), O1s (36.61%) and Ce3d5 (3.7%). The C1s peak was associated with three individual peaks at 284.3, 285.1, and 287.8 eV attributed to C–C, C–O, and C═O groups, respectively (Fig. 2b).[48] The Ce3d spectrum of the Ce-EDTA complex included two peaks at 902.8 eV and 884.6 eV attributed to the spin–orbit split into $3d_{3/2}$ and $3d_{5/2}$, respectively, which are then deconvoluted into four individual peaks (say *P*1, *P*2, *Z*1, and *Z*2) (Fig. 2c). The lower peaks at 899.5 (*Z*1) and 882.2 eV (*P*1) are assigned to the Ce $3d^9$ $4f^2$ while the higher peaks at 904.5 (*Z*2) and 885.7 eV (*P*2) are generated from the Ce $3d^9$ $4f^1$ terminal states.[52–54] This result reflects the valence state of Ce as a +III state.[54] Furthermore, the O1s was attributed to three main

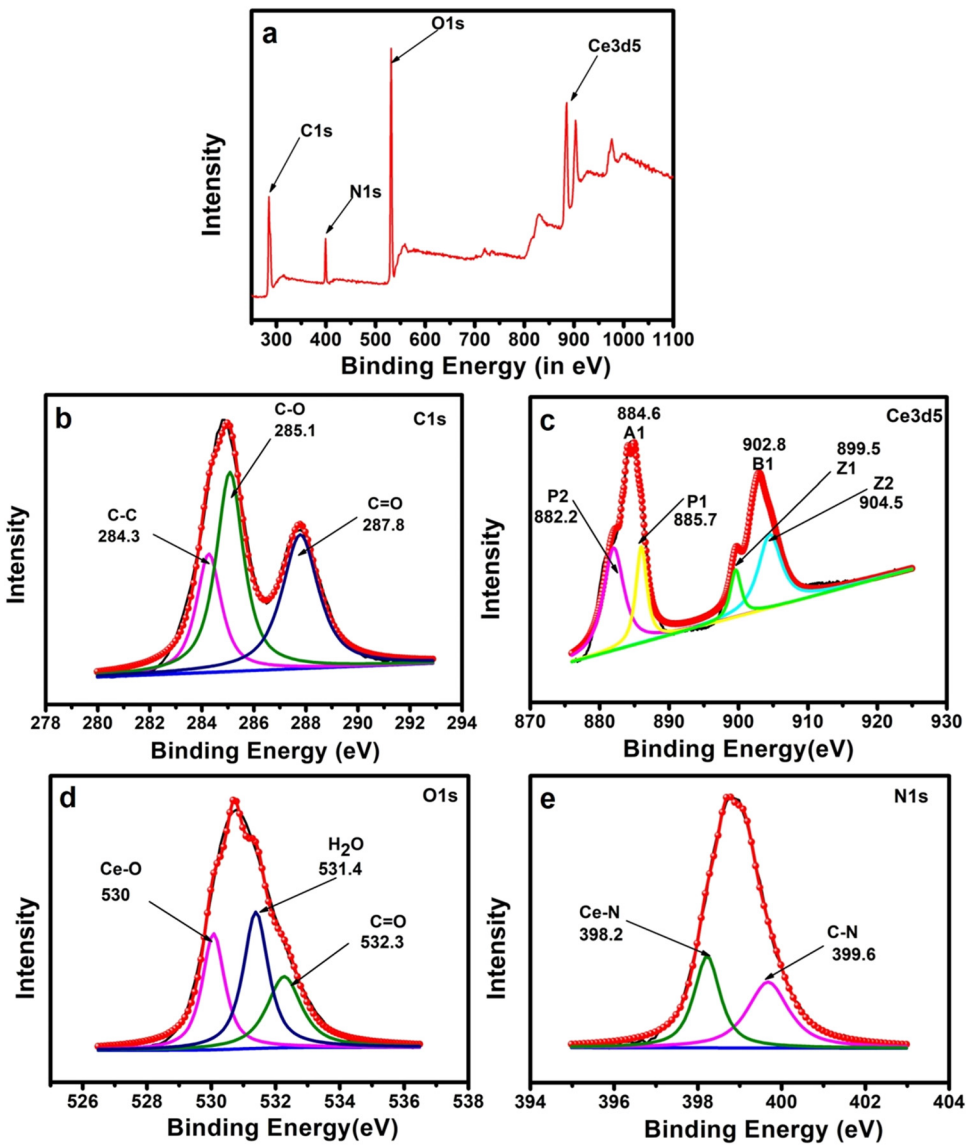

Fig. 2 XPS of (a) the survey spectrum for elemental analysis, (b) C1s, (c) Ce3d, (d) O1s and (e) N1s. Herein, the black curve is the raw data, and traced by the red curve is the fitted data corresponding to deconvoluted peaks.

peaks at 530 eV, 531.4 eV, and 532.3 eV, which are attributed to Ce–O, H_2O, and C=O (Fig. 2d).[53] Similarly, the chemical nature of the N-atom is detected in the N1s spectrum (see Fig. 1e), which is deconvoluted for two peaks at 398.2 and 399.6 eV corresponding to Ce–N and C–N bonding, respectively (Fig. 2e).[52,55–57] Based on the above characterization tools, it has been concluded that the structural and bonding features are as per the established complex as expected, as shown in Fig. 1a.

3.2 Morphological analysis

The microstructural analysis of Ce-EDTA was observed by SEM, as shown in Fig. 3a. The complex consists of polygonal microplates distributed in micron sizes with thicknesses ranging from 167.8 to 189.0 nm. These plates are distributed regularly, indicating their crystalline nature (*cf.* inset of Fig. 3a). The occurrence of all possible elements as C, N and O in the EDAX spectrum (as shown in Fig. 3b) exemplifies the existence of ligands and Ce for the central metal as expected. This means that ligand or central metal are not destroyed during its synthesis/processing conditions.

3.3 Photoluminescence analysis

Fluorescent sensors are widely utilized for the detection of biomolecules or metal ions due to their little or no destructive nature, high range of specificity, high sensitivity, ease of operation, and immunity to light scattering.[58] Taking the advantages of fluorescent quenching properties (on–off mode) or enhancing properties (off–on mode), the trace acquisition of biomolecules or ions can be monitored. Actually, in the present case study, biomolecules could quench the fluorescence phenomenon *via* energy transfer and/or electron transfer towards the fluorophores under a particular set of conditions (the detailed mechanism is discussed later).

3.3.1 Optimization of the sensing conditions. Prior to sensing, the probe is optimized for its excitation wavelength and the pH of the solution environment. The excitation-dependent photoluminescence property (PL) was noted to absorb the optimal emission characteristics of the as-synthesized Ce-EDTA complex. The material is excited for a fixed interval of excitation wavelength in this technique from 240 nm to 280 nm (Fig. 4a). We found that the emission intensity of Ce-EDTA increases first and acquires maximum intensity at 250 nm and then decreases upon further lowering the excitation energy. Similarly, the pH condition of the sensing probe is optimized by varying the pH from 4 to 10, as shown in Fig. 4b. From this figure, it is evident that the PL intensity increases with the decrease in the pH of the buffer solution. Since the pH of the physiological biological system is 7.4, the sensing of AA and Lys was performed close to physiological pH, *i.e.* pH 7, with considerable PL activity. Thus, 250 nm excitation wavelengths are optimized for the best emission intensity at pH 7 and further chosen for the detection of AA and Lys molecules. Thereafter, emission responses of Ce-EDTA were further compared with EDTA, AA, Ce-EDTA + AA and Ce-EDTA + Lys at 250 nm at pH 7 (Fig. 4c). It is evident that, under similar conditions, both the AA and EDTA exhibit poor emission spectra compared to Ce-EDTA. Herein, Ce-EDTA displays a very strong emission peak at 350 nm due to the $5d^1 \rightarrow 4f^1$ transition,[30,59] while the fluorescence intensity of Ce-EDTA is quenched on the addition of AA and Lys due to the additional interaction of these molecules as per the reaction shown in Fig. 4d. These prefatory experimental results proved that the Ce-EDTA complex has the ability to interact with AA and lysine molecules. In view of these observations, further experimentations were extended for the detection of AA and Lys.

The fluorescence responses of Ce-EDTA were recorded with the simultaneous addition of various concentrations of AA from 5.62 μM to 60.87 μM in 2 ml (100 μg ml^{-1}) Ce-EDTA at an excitation wavelength of 250 nm, as shown in Fig. 5a. We observed that as soon as the concentration of AA increases, the fluorescence activity gradually decreases. Fig. 5b represents the calibration plot between $(F_0–F/F_0)$ *vs.* concentration of AA, and shows the association of PL quenching in terms of $(F_0–F)/F_0$ with AA concentration, where F_0 is the PL intensity in the absence of AA and F is the PL intensity in the presence of AA. This plot exhibits a linear range from 11.13 to 51.92 μm corresponding to linear regression equation $(F_0–F)/F_0$ = 0.035 + 0.011 [AA] (μM) having a correlation coefficient of 0.991. The limit of detection (LOD) is evaluated as 2.04 μM (S/N = 3).

After that, we observed that Lys is also fluorescent in nature and gives distinguished emission spectra compared to Ce-EDTA even at the same excitation wavelengths (Fig. 6a). The fluorescence responses of Ce-EDTA were also recorded upon simultaneous addition of various concentrations of Lys

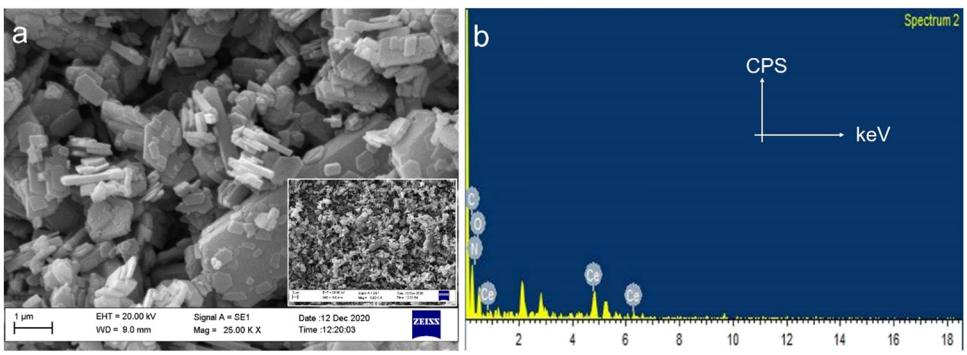

Fig. 3 (a) SEM and (b) EDAX of Ce-EDTA. The inset of Fig. 3a shows SEM of Ce-EDTA in low resolution.

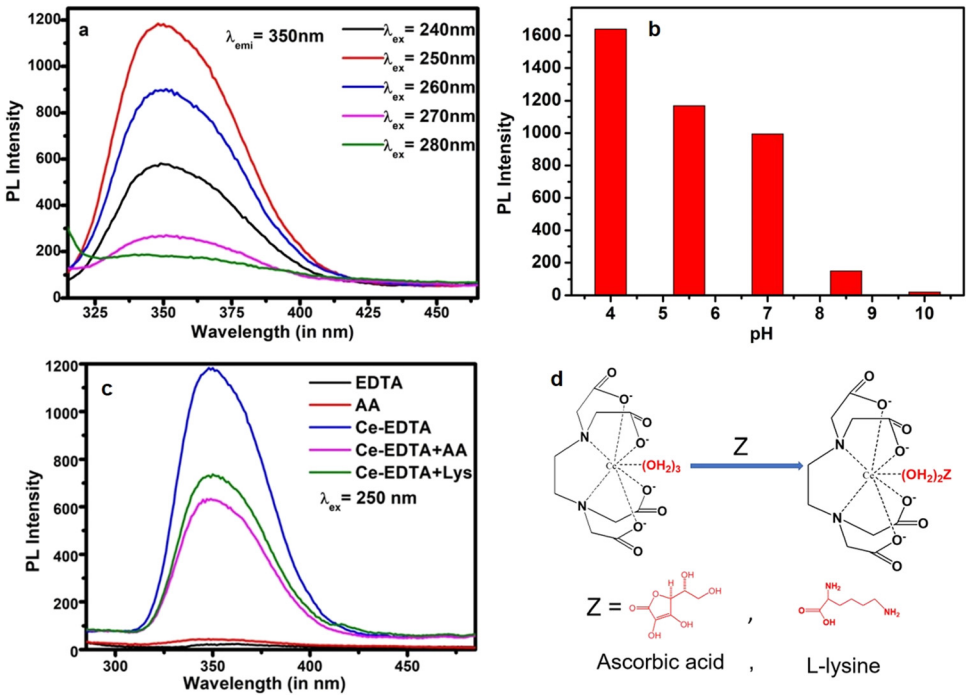

Fig. 4 (a) Response of the emission spectra of Ce-EDTA at different excitation wavelengths, (b) effect of variation of pH on the emission spectra of Ce-EDTA, (c) emission spectra of Ce-EDTA, EDTA, AA, Ce-EDTA + AA and Ce-EDTA + Lys at excitation wavelength 250 nm and (d) chemical interaction of Ce-EDTA with *Z* (= AA and Lys).

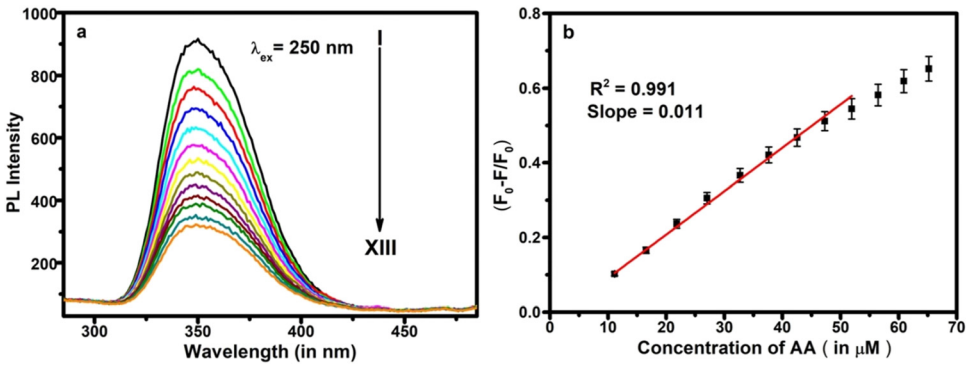

Fig. 5 (a) Response of various concentrations of AA (I → XIII as 0.00, 5.62, 11.13, 16.53, 21.82, 27.00, 32.70, 37.67, 42.53, 47.28, 51.92, 56.45 and 60.87 μM) and (b) calibration plot of $(F_0–F/F_0)$ *vs.* concentration.

from 20.29 μM to 251.74 μM at the excitation wavelength of 250 nm in 2 ml (100 μg ml^{-1}) Ce-EDTA and shown in Fig. 6b. We observed that as soon as the concentration of Lys increases, the fluorescence activity progressively decreases with minor shifting towards higher wavelengths due to the domination of the fluorescent activity of Lys.

The calibration plot exhibits a linear range from 40.19 to 151.83 μm corresponding to linear regression equation, $(F_0–F)/F_0$ = 0.083 + 0.0044 [Lys] (μM) having a correlation coefficient of 0.992. The LOD is observed here as 3.6 μM (S/N = 3).

3.3.2 Selectivity study. In order to estimate the selectivity of the technique for AA detection, some well-known common ions and compounds were selected and treated as interfering substances in the sensing approach. In this approach, the relative error was intentionally controlled within ±5% while the AA concentration was kept at 27 μM and the concentration of Lys was kept at 97.6 μM. The selectivity of the AA in the presence of different interfering agents has been tested by taking the same concentration of AA, L-glutathione (GSH), L-cystine (Cys), glycine (Gly), uric acid (UA), creatine (Cre), HPO_4^{2-}, NO_3^-, CO_3^{2-} and ten times higher concentration of Na^+, Mg^{2+}, Ca^{2+}, K^+, Mn^{2+}, Fe^{3+}, Zn^{2+} D-glucose (Glu), D-fructose (Fru), and lactose (Lac), SO_4^{2-}, and Cl^-. Among all of the interfering agents, only Gly, UA, and Cre slightly decrease the intensity of the Ce-EDTA complex due to the presence of a

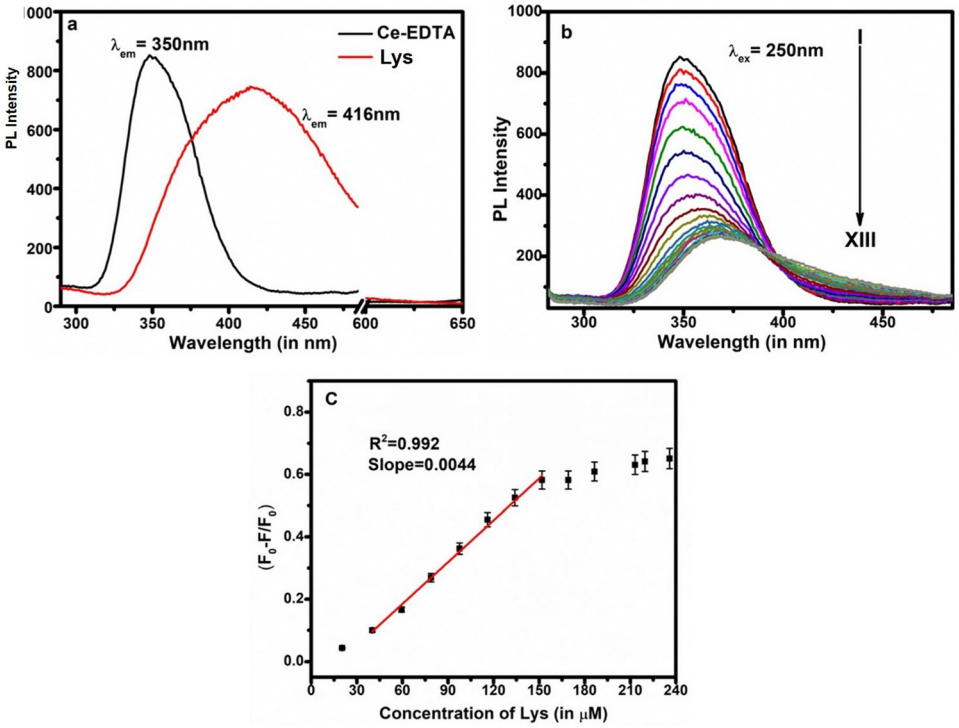

Fig. 6 (a) Emission spectra of Ce-EDTA and Lys, (b) response of various concentrations of Lys (I → XIII as 0.00, 20.29, 40.19, 59.60, 78.82, 97.60, 116, 134, 151.83, 169.24, 186.35, 213.14, and 235.83 μM) and (c) calibration plot of (F_0-F/F_0) *vs.* concentration.

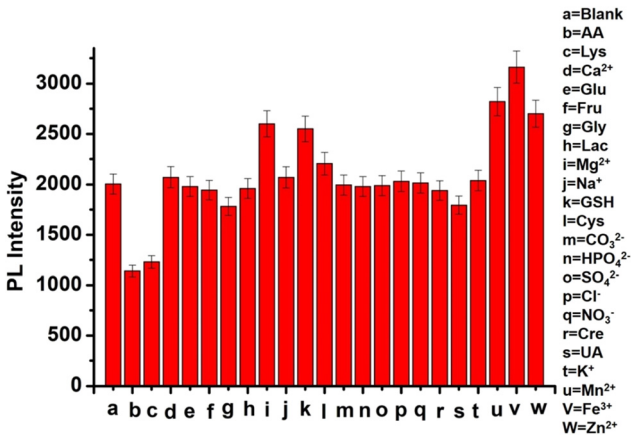

Fig. 7 Response of AA and Lys in the presence of various interferents under similar experimental circumstances.

carbonyl group that can interact with the complex like AA and Lys. GSH, Cys, Na^+, K^+, Mn^{2+}, Fe^{3+}, Zn^{2+}, Mg^{2+}, and Ca^{2+} slightly enhanced the intensity and acted as the antenna. Glu, Flu, and Lac, HPO_4^{2-}, CO_3^{2-}, SO_4^{2-}, NO_3^-, and Cl^- do not interfere with the detection of both AA and Lys. Fig. 7 exhibits the interfering outcomes of PL detection of AA and Lys under similar conditions. Moreover, the feedback of the Ce-EDTA fluorescent system to AA or Lys was not interrupted by interfering additives. Both AA and Lys showed an observable response, specifying that Ce-EDTA has good selectivity for these analytes.

3.3.3 Detection of AA and Lys in real samples. A vitamin C tablet (Celin 500 Mg) was ground into fine powder form and dissolved in 10 ml DI water with the help of sonication for 2 h. After that, the solution was centrifuged for 30 minutes at 9000 rpm, and the supernatant was pipetted out to prepare a diluted solution with 15.13 μM (70 μl supernatant and 930 μl water). Similarly, orange juice was extracted and centrifuged for 35 minutes at 10 000 rpm. After that, the filtrate was pipetted out and diluted 100 times prior to its use for AA detection. Thus, 15.13 μM AA in tablets and 33.21 μM AA in orange juice are calculated with the help of a calibration plot shown in Fig. 8b. Similarly, 1.00 g soybean seed, soaked overnight in 10 ml water, was crushed and filtered out. This extract was centrifuged for 30 minutes at 9000 rpm, and 100 μl of the supernatant was pipetted out, followed by 50 times dilution with water before use for sensing purposes. The as-prepared samples were verified and spiked for recovery analysis, and the as-observed outcomes are shown in Table 2. The spiked recoveries were acceptable for AA in fruit juice and tablets and Lys in soybean, exhibiting the appropriateness of this technique. Comparative results are summarized against the earlier works based on AA and Lys detection by various methods in Table 3. From this table, it is evident that our proposed strategy exhibits relatively better sensing properties compared to that of earlier works.

3.3.4 Sensing mechanism. In order to ensure the charge transfer, a time resolved fluorescence study was performed and the results are shown in Fig. 8a. Under excitation with a green LASER, the excited state of Ce-EDTA decays with time, and the

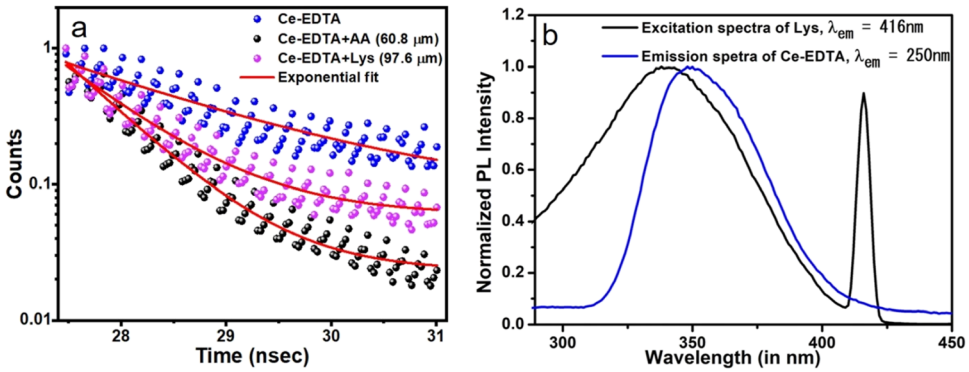

Fig. 8 (a) Fluorescence decay curve for Ce-EDTA, Ce-EDTA + AA (60.8 μm), and Ce-EDTA + Lys (97.6 μm) and (b) emission spectra of Ce-EDTA and excitation spectra of Lys.

Table 2 Recovery analyses of AA and Lys in real samples

Samples	Spiked amount (μM)	Observed concentration (μM)	% Recovery
AA in Orange juice (33.21 μM)	0	33.21	100
	5	37.65	98.53
	10	40.67	93.98
	15	43.40	90.02
AA in Tablet (15.13 μM)	0	15.13	100
	5	20.72	102.9
	10	25.59	101.8
	15	30.57	101.4
Lys in Soybean (74.93 μM)	0	74.93	100
	20	96.66	101.8
	40	106.35	92.6
	60	123.40	91.45

Table 3 Comparative study of the Ce-EDTA probe with earlier research works

	Materials	Detection technique	Quantification range (in μM)	LOD (in μM)	Ref.
Sensing of AA	Fe-CDs	Colorimetric	25–500	8.59	3
	Fe-CDs	Fluorometric	20–500	5.13	3
	AuNPs@PANI	Electrochemical	20–1600	8	60
	N,S-CDs	Fluorometric	10–200	4.69	61
	MoO_3	Colorimetric	10^3–10^5	90	62
	GQDs	Electrochemical	25–400	6.64	63
	CoTMPyP/$Sr_2Nb_3O_{10}$	Electrochemical	50–3250	10.6	64
	pHRCDs/GSH	Fluorometric	27–35	3.1	65
	GDYO-CDs	Fluorometric	10–500	2.5	66
	Ce-EDTA	Fluorometric	5.62–60.87	2.04	Present work
Sensing of Lys	GQDs/AuNPs	Fluorimetry	47–800	16.14	67
	Microbial biosensor	Dissolved oxygen spectrophotometry	10^3–10^4	1–10	68
	HPTS	Fluorimetry	0–300	3.106	69
	Ce-EDTA	Fluorometric	20.29–235.83	3.6	Present work

Note: CDs, carbon dots; NPs, nanoparticles; PANI, polyaniline; GQDs, graphene quantum dots; CoTMPyP, 5,10,15,20-tetrakis(*N*-methylpyridinium-4-yl)porphyrinato cobalt; pHRCDs, pH/redox dual sensitive fluorescent carbon dots; GDYO, Graphdiyne; HPTS, 8-hydroxypyrene-1,3,6-trisulphonic acid trisodium salt.

evolution of the fluorescence intensity with time has been recorded using an alpha 300, WITECH. Furthermore, the decay response of Ce-EDTA separately mixed with 60.8 μM of AA and 97.6 μM of Lys has also been recorded under similar measuring parameters (comparative parameters are shown in Table 4). All the decay responses have been fitted with a single exponential function, $y_t = y_t + A\exp(t/\tau)$, where A and y_0 are the curve fitting parameters, and τ represents the lifetime of the excited state of Ce-EDTA. It is observed that the lifetime of Ce-EDTA (1.6 nsec) is reduced significantly in the presence of analytes (AA and Lys). This decrease in fluorescence lifetime can be attributed to the photoinduced electron transfer (PET) from L ← M in the Ce-EDTA complex, similar to the case of the dynamic quenching mechanism. Moreover, we have also recorded the excitation spectra of Lys, keeping the emission fixed at 416 nm (as shown in Fig. 8b). It can be seen that the

Table 4 Parameters associated with different samples

Sample	Ce-EDTA	Ce-EDTA + AA (60.8 μM)	Ce-EDTA + Lys (97.6 μM)
τ (ns)	1.5599	0.59539	1.17451
Adj. *R*-Square	0.80	0.92	0.85

excitation spectra tend to overlap (>90%) with the emission spectra of the Ce-EDTA complex. Thus, the fluorescence quenching of Ce-EDTA with increasing Lys concentration can be explained in terms of the fluorescence resonance energy transfer (FRET) mechanism, where the emission from the fluorophore causes excitation of the analyte molecules through a non-radiative energy transfer.

4. Conclusions

We synthesized a fluorescent probe based on a Ce-EDTA complex compound with monoclinic and triclinic crystal phases with low symmetric ties from the most abundant rare earth Ce-metal and EDTA ligands by a hydrothermal process. In this compound, three labile H_2O molecules are observed, including chelation of hexadentate EDTA. This labile H_2O is prone to bind either kind of carboxyl moiety and hence the consequence of AA and Lys detection in concentration ranges from 5.62 to 60.87 μM and 20.29 to 235.83 μM, respectively. Similarly, the LODs of AA and Lys were observed as 2.04 and 3.6 μM. Sensing of these analytes was achieved through the FRET mechanism. Our as-synthesized probe is well suited for sensing of AA and Lys in the presence of various interferents. It is also applicable to detect AA in orange juice, and ascorbic acid tablets, and Lys in soybean seed.

Author contributions

Rajpal: data curation, formal analysis, methodology, validation, writing – original draft; Ashish Kumar: formal analysis, methodology, validation, writing – review & editing; Subhajit Jana: XRD analysis and drafting, writing – review & editing; Priya Singh: data curation, formal analysis; Rajiv Prakash: conceptualization, project administration, resources, supervision.

Conflicts of interest

The authors declare no competing financial interest.

Acknowledgements

The authors are thankful to Dr Chandan Upadhyay, School of Materials Science and Technology (SMST), IIT (BHU), for providing the PL characterization facility. Rajpal is thankful to the Council of Scientific and Industrial Research (CSIR), New Delhi, India (File no. 09/1217(0051)/2018-EMR-1) for his fellowship. The authors are also thankful to the Central Instrument Facility, IIT (BHU), for SEM, XRD, UV-Visible spectroscopy, and FT-IR facilities.

References

1 J. Zhang, R. Chen, Q. Chen, Y. Hu, S. Pan and X. Hu, Ratiometric fluorescent probe for ascorbic acid detection based on MnO_2 nanosheets, gold nanoclusters and thiamine, *Colloids Surf., A*, 2021, **622**, 126605.

2 L. Zhi, M. Li, S. Zhang, J. Tu and X. Lu, One stone with four birds: Methylene blue decorated oxygen-vacancy-rich MnO_2 nanosheets for multimode detection of ascorbic acid, *Sens. Actuators, B*, 2022, **354**, 131106.

3 P. Fan, C. Liu, C. Hu, F. Lin, S. Yang and F. Xiao, Green and facile synthesis of iron-doped biomass carbon dots as a dual-signal colorimetric and fluorometric probe for the detection of ascorbic acid, *New J. Chem.*, 2022, **46**, 2526–2533.

4 L. Wang, C. Gong, Y. Shen, W. Ye, M. Xu and Y. Song, A novel ratiometric electrochemical biosensor for sensitive detection of ascorbic acid, *Sens. Actuators, B*, 2017, **242**, 625–631.

5 X. Gao, X. Zhou, Y. Ma, T. Qian, C. Wang and F. Chu, Facile and cost-effective preparation of carbon quantum dots for Fe^{3+} ion and ascorbic acid detection in living cells based on the ''on-off-on'' fluorescence principle, *Appl. Surf. Sci.*, 2019, **469**, 911–916.

6 Y. Lyu, Z. Tao, X. Lin, P. Qian, Y. Li, S. Wang and Y. Liu, A MnO_2 nanosheet-based ratiometric fluorescent nanosensor with single excitation for rapid and specific detection of ascorbic acid, *Anal. Bioanal. Chem.*, 2019, **411**, 4093–4101.

7 T. Sun, S. Hao, R. Fan, J. Zhang, W. Chen, K. Zhu, P. Wang, X. Fang and Y. Yang, *In situ* self-assembled cationic lanthanide metal organic framework membrane sensor for effective MnO_4^- and ascorbic acid detection, *Anal. Chim. Acta*, 2021, **1142**, 211–220.

8 A. Wu, H. Ding, W. Zhang, H. Rao, L. Wang, Y. Chen, C. Lu and X. Wang, A colorimetric and fluorescence turn-on probe for the detection of ascorbic acid in living cells and beverages, *Food Chem.*, 2021, **363**, 130325.

9 J. Peng, J. Ling, X.-Q. Zhang, L.-Y. Zhang, Q.-E. Cao and Z.-T. Ding, A rapid, sensitive and selective colorimetric method for detection of ascorbic acid, *Sens. Actuators, B*, 2015, **221**, 708–716.

10 D. Yue, D. Zhao, J. Zhang, L. Zhang, K. Jiang, X. Zhang, Y. Cui, Y. Yang., B. Chen and G. Qian, A luminescent cerium metal–organic framework for the turn-on sensing of ascorbic acid, *Chem. Commun.*, 2017, **53**, 11221–11224.

11 A. Mazurek and J. Jamroz, Precision of dehydroascorbic acid quantitation with the use of the subtraction method-Validation of HPLC–DAD method for determination of total vitamin C in food, *Food Chem.*, 2015, **173**, 543–550.

12 M. Levine, K. R. Dhariwal, P. W. Washko, J. D. Butler, R. W. Welch, Y. H. Wang and P. Bergsten, Ascorbic acid and in situ kinetics: a new approach to vitamin requirements, *Am. J. Clin. Nutr.*, 1991, **54**, 1157S–1162S.

13 A. Bikker, J. Wielders, R. V. Loo and M. Loubert, Ascorbic acid deficiency impairs wound healing in surgical patients: Four case reports, *Int. J. Surg. Open*, 2016, **2**, 15–18.

14 J.-J. Liu, Z.-T. Chen, D.-S. Tang, Y.-B. Wang, L.-T. Kang and J.-N. Yao, Graphene quantum dots-based fluorescent probe for turn-on sensing of ascorbic acid, *Sens. Actuators, B*, 2015, **212**, 214–219.

15 T. Dimitrijevic, P. Vulic, D. Manojlović, A. S. Nikolic and D. M. Stankovic, Amperometric ascorbic acid sensor based on doped ferrites nanoparticles modified glassy carbon paste electrode, *Anal. Biochem.*, 2016, **504**, 20–26.

16 M. Levine, Y. Wang, S. J. Padayatty and J. Morrow, A new recommended dietary allowance of vitamin C for healthy young women, *Proc. Natl. Acad. Sci. U. S. A.*, 2001, **98**, 9842–9846.

17 J. M. Rivers, Safety of high-level vitamin C ingestion, *Int. J. Vitam. Nutr. Res., Suppl.*, 1989, **30**, 95–102.

18 J. N. Hathcock, A. Azzi, J. Blumberg, T. Bray, A. Dickinson, B. Frei, I. Jialal, C. S. Johnston, F. J. Kelly, K. Kraemer, L. Packer, S. Parthasarathy, H. Sies and M. G. Traber, Vitamins E and C are safe across a broad range of intakes, *Am. J. Clin. Nutr.*, 2005, **81**(4), 736–745.

19 C. Guo, Q. Jin, Y. Y. Wang, B. Ding, Y. Li, J. Huo and X. Zhao, Developing a unique metal-organic framework-{[$Cd(abtz)_2$-(NCS)]·(ClO_4)}*n* (abtz = 1-(4-aminobenzyl)-1,2,4-triazole) as fluorescent probe for highly selective and sensitive detection of ascorbic acid in biological liquid, *Sens. Actuators, B*, 2016, **234**, 184–191.

20 Y. Yang, W. Zhu, B. Sun, H. Hu, X. Li, S. Bao and Z. Su, Two fluorescent cerium metal-organic frameworks for the ''turn-on'' sensing of AA with high sensitivity as well as biological and electrochemical properties, *J. Solid State Chem.*, 2021, **302**, 122376.

21 L. Li, C. Wang, K. Liu, Y. Wang, K. Liu and Y. Lin, Hexagonal Cobalt Oxyhydroxide–Carbon Dots Hybridized Surface: High Sensitive Fluorescence Turn-on Probe for Monitoring of Ascorbic Acid in Rat Brain Following Brain Ischemia, *Anal. Chem.*, 2015, **87**, 3404–3411.

22 M. Iwasaki, J. Ishihara, R. Takachi, H. Todoriki, H. Yamamoto, H. Miyano, T. Yamaji and S. Tsugane, Validity of a self-administered food-frequency questionnaire for assessing amino acid intake in Japan: comparison with intake from 4-day weighed dietary records and plasma levels, *J. Epidemiol.*, 2016, **26**(1), 36–44.

23 E. Fjellstedt, L. Harnevik, J.-O. Jeppsson, H.-G. Tiselius, P. Soderkvist and T. Denneberg, Urinary excretion of total cystine and the dibasic amino acids arginine, lysine and ornithine in relation to genetic findings in patients with cystinuria treated with sulfhydryl compounds, *Urol. Res.*, 2003, **31**, 417–425.

24 J. Dancis, J. Hutzler, M. G. Ampola, V. E. Shih, H. H. Van Gelderen, L. T. Kirby and N. C. Woody, The Prognosis of Hyperlysinemia: An Interim Report, *Am. J. Hum. Genet.*, 1983, **35**, 438–442.

25 F. Preuschoff, U. Spohn and D. Janasek, Photodiode-based chemiluminometric biosensors for hydrogen peroxide and L-lysine, *Biosens. Bioelectron.*, 1994, **9**, 543–549.

26 V. R. Pavithra, T. D. Thangadurai, G. Manonmani, K. Senthilkumar, D. Nataraj, J. Jiya, K. Nandakumar and S. Thomas, Investigation on surface interaction between graphene nanobuds and cerium(III) *via* fluorescence excimer, theoretical, real water sample, and bioimaging studies, *Mater. Chem. Phys.*, 2021, **264**, 124453.

27 A. F. Kateshali, S. G. Dogaheh, J. Soleimannejad and A. J. Blake, Structural diversity and applications of Ce(III)-based coordination polymers, *Coord. Chem. Rev.*, 2020, **419**, 213392.

28 S. A. Younis, N. Bhardwaj, S. K. Bhardwaj, K.-H. Kim and A. Deep, Rare earth metal–organic frameworks (RE-MOFs): Synthesis, properties, and biomedical applications, *Coord. Chem. Rev.*, 2021, **429**, 213620.

29 M. N. Akhtar, M. Mateen, M. Sadakiyo, M. F. Warsi, M. A. AlDamen and Y. Song, 1D cerium(III) coordination polymer with pivalate bridges: Synthesis, structure and magnetic properties, *J. Mol. Struct.*, 2017, **1141**, 170–175.

30 I. L. Malaestean, M. K-Alıcı, A. Ellern, J. V. Leusen, H. Schilder, M. Speldrich, S. G. Baca and P. Kogerler, Linear, Zigzag, and Helical Cerium(III) Coordination Polymers, *Cryst. Growth Des.*, 2012, **12**, 1593–1602.

31 Z. Shen, S. He, P. Yao, X. Lao, B. Yang, Y. Dai, X. Sun and T. Chen, Lanthanum-based coordination polymers microplates using a ''green ligand'' EDTA with tailorable morphology and fluorescent property, *RSC Adv.*, 2014, **4**, 12844–12848.

32 M. Yang, T. Chen, Z. Wei, M. Li, H. Bi, Q. Zeng, Z. Shen and Y. Shen, Hyperbranched microspheres formed by an EDTA-based coordination polymer with ternary architectures assembled by ultrathin nanoribbons and their tricolor luminescent properties, *CrystEngComm*, 2012, **14**, 3653–3657.

33 T. Yi, S. Gao and B. Li, Edta-linked 4f-3d heterometallic two-dimensional sheet in Ln_2M_3 $(edta)_3$ $(H_2O)_{11}{\cdot}12H_2O$ (Ln = Nd, Gd; M = Mn, Co), *Polyhedron*, 1998, **17**, 2243–2248.

34 R. S. Shukla, S. D. Bhatt, R. B. Thorat and R. V. Jasra, A novel effective hydration of carbon monoxide in liquid phase by a water-soluble ruthenium complex catalyst at moderate pressures in aqueous medium, *Appl. Catal., A*, 2005, **294**, 111–118.

35 H. Liu, L. Xu, G.-G. Gao, F.-Y. Li, Y.-Y. Yang, Z.-K. Li and Y. Sun, Two-dimensional layer architecture assembled by Keggin polyoxotungstate, Cu (II)–EDTA complex and sodium linker: Synthesis, crystal structures, and magnetic properties, *J. Solid State Chem.*, 2007, **180**, 1664–1671.

36 K. Sasaki, S. Oguma, Y. Namiki and N. Ohmura, Monoclonal Antibody to Trivalent Chromium Chelate Complex and Its Application to Measurement of the Total Chromium Concentration, *Anal. Chem.*, 2009, **81**, 4005–4009.

37 F. Yang, Z. Yu, X. Li, P. Ren, G. Liu, Y. Song and J. Wang, Design and synthesis of a novel lanthanide fluorescent probe (TbIII-dtpa-bis(2,6-diaminopurine)) and its application to the detection of uric acid in urine sample, *Spectrochim. Acta, Part A*, 2018, **203**, 461–471.

38 Y. Song, J. Chen, D. Hu, F. Liu, P. Li, H. Li, S. Chen, H. Tan and L. Wang, Ratiometric fluorescent detection of biomakers for biological warfare agents with carbon dots

chelated europium-based nanoscale coordination polymers, *Sens. Actuators, B*, 2015, **221**, 586–592.

39 Y. Chen, Y. Chi, H. Wen and Z. Lu, Sensitized Luminescent Terbium Nanoparticles: Preparation and Time-Resolved Fluorescence Assay for DNA, *Anal. Chem.*, 2007, **79**, 960–965.

40 H. Tan, Y. Zhang and Y. Chen, Detection of mercury ions (Hg^{2+}) in urine using a terbium chelate fluorescent probe, *Sens. Actuators, B*, 2011, **156**, 120–125.

41 Y. Chen, X. Jin and C. Sun, Ultrasensitive fluorescence detection of bismuth ion(III) in plasma, urine and medicines by a terbium chelate probe, *Sens. Actuators, B*, 2021, **331**, 129439.

42 W.-B. Tseng, Y.-T. Lu, S.-W. Zhan and W.-L. Tseng, Self-assembly of c-di-GMP, Tb^{3+}, and Ag^{+} into high-quantum-yield coordination polymer nanoparticles: Mechanism discussion and application as a c-di-GMP sensor, *Sens. Actuators, B*, 2020, **312**, 127960.

43 F. Pu, S. Qu, H. Qiu and L. Zhang, Regulation of light-harvesting antenna based on silver ion-enhanced emission of dye-doped coordination polymer nanoparticles, *J. Colloid Interface Sci.*, 2020, **578**, 254–261.

44 M.-L. Chen, S. Gao and Z.-H. Zhou, Isolations and characterization of highly water-soluble dimeric lanthanide citrate and malate with ethylenediaminetetraacetate, *Dalton Trans.*, 2012, **41**, 1202–1209.

45 P. Glentworth, B. Wiseall, C. L. Wright and A. J. Mahmood, A kinetic study of isotopic exchange reactions between lanthanide ions and lanthanide polyaminopolycarboxylic acid complex ions-I isotopic exchange reactions of Ce(III) with Ce (HEDTA), Ce $(EDTA)^{-}$, Ce $(DCTA)^{-}$ and Ce $(DTPA)2^{-}$, *J. Inorg. Nucl. Chem.*, 1968, **30**, 967–986.

46 J. A. Bogart, A. J. Lewis and E. J. Schelter, DFT Study of the Active Site of the XoxF-Type Natural, Cerium-Dependent Methanol Dehydrogenase Enzyme, *Chem. – Eur. J.*, 2015, **21**, 1743–1748.

47 C. S. Stan, I. Rosca, D. Sutiman and M. S. Secula, Highly luminescent europium and terbium complexes based on succinimide and *N*-hydroxysuccinimide, *J. Rare Earths*, 2012, **30**, 401.

48 K. C. Lanigan and K. Pidsosny, Reflectance FTIR spectroscopic analysis of metal complexation to EDTA and EDDS, *Vib. Spectrosc.*, 2007, **45**, 2–9.

49 X. F. Wanga, J. Wang, J. Gao, Y. F. Wang, Z. Q. Xing, R. Xu, G. R. Gao and X. D. Zhang, Syntheses and Structural Determination of the Nine-coordinate Rare Earth Metal Complexes: $[Tb^{III}(Eg3a)(H_2O)_2]\cdot 4.5H_2O$ and $K[Tb^{III}(Edta)\text{-}(H_2O)_3]\cdot 5H_2O^1$, *Russ. J. Coord. Chem.*, 2008, **34**, 350–359.

50 I. Ameen, A. K. Tripathi, R. L. Mishra, A. Siddiqui and U. N. Tripathi, Luminescent, optical, magnetic and meta-material behavior of cerium complexes, *J. Saudi Chem. Soc.*, 2019, **23**, 725–739.

51 C. Canevali, M. Mattoni, F. Morazzoni, R. Scotti, M. Casu, A. Musinu, R. Krsmanovic, S. Polizzi, A. Speghini and M. Bettinelli, Stability of Luminescent Trivalent Cerium in Silica Host Glasses Modified by Boron and Phosphorus, *J. Am. Chem. Soc.*, 2005, **127**, 14681–14691.

52 K. Kim, Y. Kim and J. Kim, Enhanced cathodic catalytic activity of an N-doped micropore structure obtained through the six-coordinate bond of an EDTA-Ce composite for the oxygen reduction reaction, *Appl. Surf. Sci.*, 2020, **505**, 144418.

53 J.-L. Yang, Y.-J. Li, Y.-H. Yuan, R.-P. Liang and J.-D. Qiu, Target induced aggregation of Ce(III) - based coordination polymer nanoparticles for fluorimetric detection of As(III), *Talanta*, 2018, **190**, 255–262.

54 A. Perez, R. Molina and S. Moreno, Enhanced VOC oxidation over Ce/CoMgAl mixed oxides using a reconstruction method with EDTA precursors, *Appl. Catal., A*, 2014, **477**, 109–116.

55 A. B. Jorge, Y. Sakatani, C. Boissiere, C. L-Roberts, G. Sauthier, J. Fraxedas, C. Sanchez and A. Fuertes, Nanocrystalline N-doped ceria porous thin films as efficient visible-active photocatalysts, *J. Mater. Chem.*, 2012, **22**, 3220.

56 Z. Liu, X. Hao, Y. Li and X. Zhang, Novel Ce @ N-CDs as green corrosion inhibitor for metal in acidic environment, *J. Mol. Liq.*, 2022, **349**, 118155.

57 D. Liu, Y. Liu, Z. Wu, F. Tian, B.-C. Ye and X. Chen, Enhancement of photodegradation of Ce, N, and P tri-doped TiO_2/AC by microwave radiation with visible light response for naphthalene, *J. Taiwan Inst. Chem. Eng.*, 2016, **68**, 506–513.

58 W. Fang, K. Liu, G. Wang, Y. Liang, R. Huang, T. Liu, L. Ding, J. Peng, H. Peng and Y. Fang, Dual-phase emission AIEgen with ICT properties for VOC chromic sensing, *Anal. Chem.*, 2021, **93**, 8501–8507.

59 T. Murata, M. Sato, H. Yoshida and K. Morinaga, Compositional dependence of ultraviolet fluorescence intensity of Ce^{3+} in silicate, borate, and phosphate glasses, *J. Non-Cryst. Solids*, 2005, **351**, 312–316.

60 L. Yang, S. Liu, Q. Zhang and F. Li, Simultaneous electrochemical determination of dopamine and ascorbic acid using AuNPs @ polyaniline core–shell nanocomposites modified electrode, *Talanta*, 2012, **89**, 136–141.

61 X. Luo, W. Zhang, Y. Han, X. Chen, L. Zhu, W. Tang, J. Wang, T. Yue and Z. Li, N, S co-doped carbon dots-based fluorescent ''on-off-on'' sensor for determination of ascorbic acid in common fruits, *Food Chem.*, 2018, **258**, 214–221.

62 R. Li, H. An, W. Huang and Y. He, Molybdenum oxide nanosheets meet ascorbic acid: Tunable surface plasmon resonance and visual colorimetric detection at room temperature, *Sens. Actuators, B*, 2018, **259**, 59–63.

63 K. Kunpatee, S. Traipop, O. Chailapakul and S. Chuanuwatanakul, Simultaneous determination of ascorbic acid, dopamine, and uric acid using graphene quantum dots/ionic liquid modified screen-printed carbon electrode, *Sens. Actuators, B*, 2020, **314**, 128059.

64 S. Wu, T. Sun, H. Wang, Z. Fan, L. Li, B. Fan, L. Liu, J. Ma and Z. Tong, A sandwich-structured, layered CoTMPyP/$Sr_2Nb_3O_{10}$ nanocomposite for simultaneous voltametric determination of dopamine and ascorbic acid, *J. Electroanal. Chem.*, 2020, **873**, 114403.

65 P. Zhu, Y. Gan, K. Lin, C. Lin, S. Li, S. Yu and J. Shi, Dual-Response Detection of Oxidized Glutathione, Ascorbic Acid, and Cell Imaging Based pH/Redox Dual-Sensitive Fluorescent Carbon Dots, *ACS Omega*, 2020, **5**, 4482–4489.

66 Q. Bai, C. Zhang, L. Li, Z. Zhu, L. Wang, F. Jiang, M. Liu, Z. Wang, W. W. Yu, F. Du, Z. Yang and N. Sui, Subsequent monitoring of ferric ion and ascorbic acid using graphdiyne quantum dots-based optical sensors, *Microchim. Acta*, 2020, **187**, 657.

67 C. Chaicham, T. Tuntulani, V. Promarak and B. Tomapatanaget, Effective GQD/AuNPs nanosensors for selectively bifunctional detection of lysine and cysteine under different photophysical properties, *Sens. Actuators, B*, 2019, **282**, 936–944.

68 E. Akyilmaz, A. Erdogan, R. Ozturk and I. Yasa, Sensitive determination of l-lysine with a new amperometric microbial biosensor based on Saccharomyces cerevisiae yeast cells, *Biosens. Bioelectron.*, 2007, **22**, 1055–1060.

69 R. S. Bhosale, G. V. Shitre, R. Kumar, D. O. Biradar, S. V. Bhosale, R. Narayan and S. V. Bhosale, A 8-hydroxypyrene-1,3,6-trisulfonic acid trisodium salt (HPTS) based colorimetric and green turn-on fluorescent sensor for the detection of arginine and lysine in aqueous solution, *Sens. Actuators, B*, 2017, **241**, 1270–1275.